Applied Physics A (2018) 124:849
https://doi.org/10.1007/s00339-018-2255-4

Applied Physics A
Materials Science & Processing

Influence of tungsten carbide (WC) nanoparticle on microstructure and mechanical properties of Cu/Sn57.6Bi0.4Ag/Cu solder joints

Li Yang[1,2] · Guoqiang Wang[1,2] · Yaocheng Zhang[1] · Yifeng Xiong[1,2] · Wei Jiang[1,2]

Received: 23 August 2018 / Accepted: 15 November 2018 / Published online: 28 November 2018
© Springer-Verlag GmbH Germany, part of Springer Nature 2018

Abstract
The effect of WC nanoparticles on the spreadability, microstructure and mechanical properties of Cu/Sn57.6Bi0.4Ag/Cu solder joints was investigated. The results showed that the spreadability of Sn57.6Bi0.4Ag composite solder was enhanced by WC nanoparticles, and the spreadability was increased first and decreased with increasing WC content next; when the content of WC was 0.1 wt%, the solder got relatively optimal spreadability. The dispersed WC particles provided the heterogeneous nucleation sites during the soldering process and led to the microstructure refinement of Sn57.6Bi0.4Ag solder alloy. WC particles restrained the growth rate of IMC by reducing the surface energy of Cu_6Sn_5, the shear strength of Sn57.6Bi0.4Ag–xWC/Cu ($x=0$, 0.1) solder joints decreased seriously with increasing aging time, WC particles improved the shear strength and toughness of Sn57.6Bi0.4Ag/Cu solder joints by refining the microstructure.

1 Introduction

In recent years, many researchers have proposed lead-free solder alloys to substitute the lead-containing solder alloys, such as Sn–Ag–Cu, Sn–Ag, Sn–Cu, Sn–Zn and Sn–Bi [1–5]. The melting points of new lead-free solders were significantly higher than that of SnPb solder, and commonly used in wave soldering and reflow soldering techniques [6–8], among which Sn58Bi solder was one of the most promising alternatives. The performance of Sn58Bi solder alloy was significantly improved by silver (Ag). Li et al. [9] investigated the effect of Ag nanoparticle size on the growth behavior of solder/Cu interfacial intermetallic compounds (IMCs) and shear strength of Sn58Bi joint, and found that Ag played a positive role in improving the mechanical properties of Sn58Bi solder, the improvement varied with the Ag particle size. Sun et al. [10] investigated the influence of the Ag_3Sn on the electromigration phenomenon in the Ag-doped Sn58Bi solder joints, and found that grain refinement caused by Ag element was the main reason for the electromigration improvement. Sn57.6Bi0.4Ag solder had the advantages of Sn58Bi solder, such as low melting point, good spreadability and excellent mechanical properties. The interface of Cu/Sn57.6Bi0.4Ag/Cu solder joint was relatively rough compared to that of Cu/Sn58Bi/Cu joints, the shear strength of Cu/Sn57.6Bi0.4Ag/Cu joints was significantly higher than that of Cu/Sn58Bi/Cu joints [11]. Sn57.6Bi0.4Ag solder has excellent effects in practical applications and environmental protection, while the brittleness of Sn57.6Bi0.4Ag solder caused serious deterioration in processing performance and service performance [12].

One of the strategies that aim at improving solder joint reliability is adding strengthening particles. The strengthening particles in solder blocked grain boundary movement, hindered lattice dislocation, formed a well-characterized IMC and improved the stability of solder alloy joints in the temperature, force and electric fields [13–15]. In the case of Sn57.6Bi0.4Ag solder, Lee et al. [16] found that the mechanical properties of Sn57.6Bi0.4Ag solder alloy were improved by Pd, Co, Zn and Ni. Li et al. [17] found that Sn57.6Bi0.4Ag solder was reinforced successfully through the tungsten (W) nanoparticles at a concentration of 0.5 wt%, the lamellar interphase spacing of the solder matrix was reduced by 31.0%, and the shear strength of Sn57.6Bi0.4Ag/Cu solder joint was increased by 8.2%. Sun et al. [18] found that the mechanical properties of Sn57.6Bi0.4Ag solder joints could be improved by CNTs and Ni–CNTs; the fractured surface of Sn57.6Bi0.4Ag solder joints was relatively rough and showed better bonding performance.

✉ Li Yang
yangli2011@cslg.edu.cn

[1] School of Automotive Engineering, Changshu Institute of Technology, Jiangsu 215500, People's Republic of China

[2] School of Mechanical and Electrical Engineering, Soochow University, Jiangsu 215000, People's Republic of China

Previous studies showed that CNTs, Pd, W and other reinforcing particles have different influences on the spreadability and shear property of Sn57.6Bi0.4Ag solders. Hu et al. [19] found that the addition of Al_2O_3 (ceramic particles) significantly hindered the reduction of shear strength of SnBi/Cu solder joints after 48 h and 288 h of aging. WC (ceramic particles) has excellent physical and mechanical properties, such as ultimate tensile strength of 344 MPa, compressive strength of 2683–2958 MPa, hardness of 90 RA, Young's modulus of 668 GPa and melting point of 2777 °C [20, 21]. In this paper, the effects of WC particles on the melting behavior, spreadability, microstructure and mechanical properties of Sn57.6Bi0.4Ag solder joints were investigated.

2 Experimental procedures

Sn57.6Bi0.4Ag solder paste was provided by Alpha Advanced Materials. The nano-WC particle (as shown in Fig. 1) (purity 99%) with an average diameter of 80 nm was added into the Sn57.6Bi0.4Ag solder. Sn57.6Bi0.4Ag–xWC solder pastes were prepared by sufficient mechanical stirring. The nominal chemical composition of the five Sn57.6Bi0.4Ag composite solder alloys is listed in Table 1.

The melting behavior of Sn57.6Bi0.4Ag–xWC ($x=0$, 0.025, 0.050, 0.100, 0.200) composite solder alloys was investigated by differential scanning calorimetry (Shimadzu DSC-50) analyzer with heating rate of 5 °C/min. About 0.23 g each solder alloy was melt in the Cu sheets and then the spreading area was measured after reflowing by F4N reflow machine at 200 °C for 5 min, each experimental condition was evaluated as the average of five replicate tests for each solder. Scanning electron microscopy (SEM) was used to collect the microstructure and IMC layer of the solder alloys; energy-dispersive spectroscopy (EDS) was applied to detect the elemental distribution of the solder alloys. The average thickness of the IMC layers of Sn57.6Bi0.4Ag–xWC ($x=0$, 0.1) joint was calculated by the following equation [22]:

Table 1 Nominal chemical composition of the SnBiAg base composite solders (wt%)

Solder	Bi	Ag	WC	Sn
SnBiAg	57.6	0.4	0	Bal
SnBiAg–0.025WC	57.6	0.4	0.025	Bal
SnBiAg–0.05WC	57.6	0.4	0.05	Bal
SnBiAg–0.1WC	57.6	0.4	0.1	Bal
SnBiAg–0.2WC	57.6	0.4	0.2	Bal

$$T = \frac{\sum_{i=1}^{n} t_i}{n}, \tag{1}$$

where t_i was the IMC layer thickness at different positions on the interface, n was the measurement times, and T was the average IMC layer thickness.

The solder/Cu joints were prepared by reflowing and then solidified by air-cooling; the dimensions of the shear specimen were 20 mm × 1 mm × 1 mm. The Sn57.6Bi0.4Ag/Cu and Sn57.6Bi0.4Ag–0.1WC/Cu solder joints were aged using a convection reflow oven (BTU PYRAMAX 100 N) at 100 °C for 250 h, 500 h and 1000 h, respectively. The shear strength of Sn57.6Bi0.4Ag–xWC/Cu ($x=0$, 0.1) solder joints was carried out by PTR1102 bonding strength tester with stretching rate of 0.4 mm/s. The shear fracture of Sn57.6Bi0.4Ag–xWC/Cu ($x=0$, 0.1) solder joints was observed by SEM.

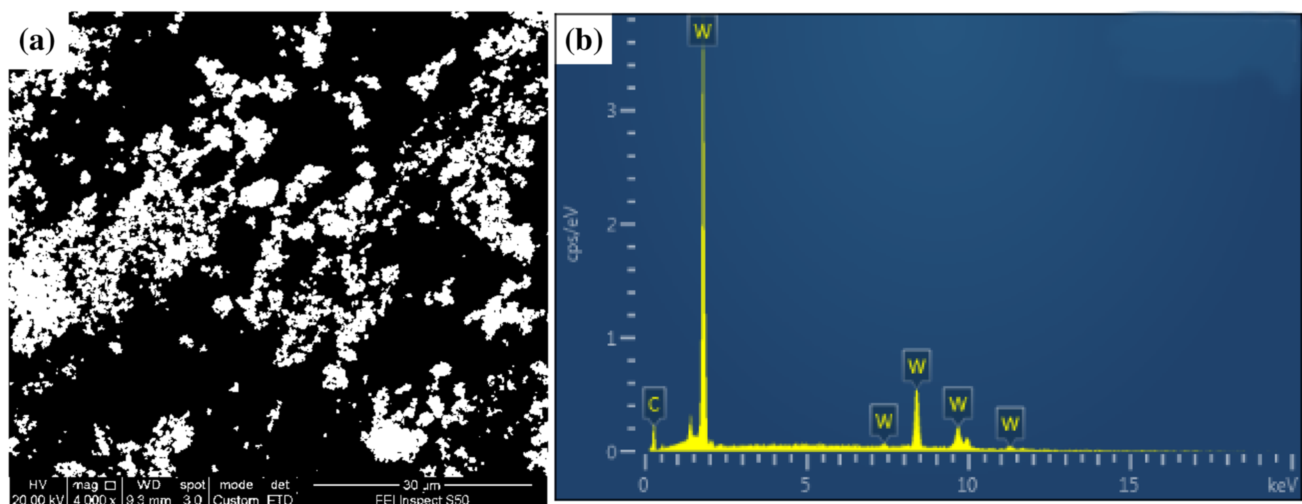

Fig. 1 **a** Morphology and **b** EDS spectrum of the WC nanoparticles

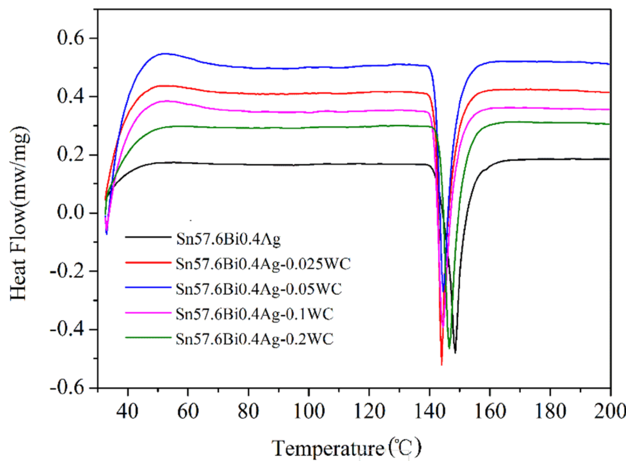

Fig. 2 DSC curves of Sn57.6Bi0.4Ag–*x*WC ($x=0$, 0.025, 0.050, 0.100, 0.200) solder alloys

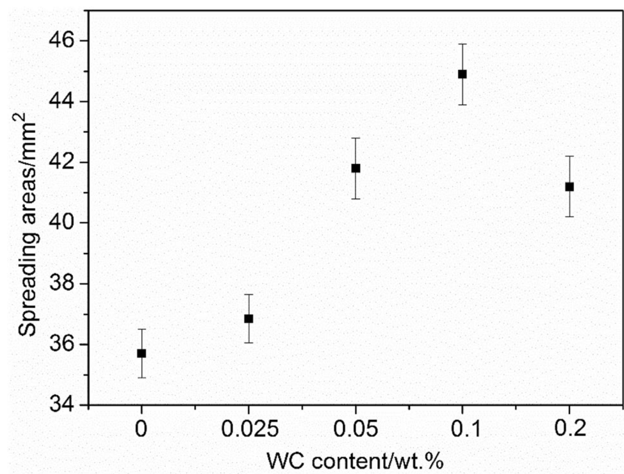

Fig. 3 Effect of WC particles on spreading areas of Sn57.6Bi0.4Ag solder alloys

3 Results and discussion

3.1 Melting point

Figure 2 shows the DSC curves of Sn57.6Bi0.4Ag–*x*WC ($x=0$, 0.025, 0.050, 0.100, 0.200) composited solder alloy. The melting temperatures of Sn57.6Bi0.4Ag–*x*WC ($x=0$, 0.025, 0.050, 0.100, 0.200) solder alloys are maintained at 145 ± 2 °C in most cases. There are no significant differences in the melting temperature among the five solders. The trace amount of WC particles into Sn57.6Bi0.4Ag solder alloy does not apparently affect the melting temperature of Sn57.6Bi0.4Ag solder alloy. Generally, the melting property is an inherent physical property of the material, the addition of nanoparticles has little impact on the melting temperature. The results are similar to previous reports for composite solders [23, 24].

3.2 Spreadability

The relationship between the spreading areas and the WC proportion in the solder joints is shown in Fig. 3. The spreadability of Sn57.6Bi0.4Ag solder is improved by nano-WC particles, the tendency of the spreadability of the solder alloy can be summarized to be increase first and decrease with increasing WC content next. The spreading area of Sn57.6Bi0.4Ag solder is 35.7 mm^2, and it reaches 44.9 mm^2 when the addition amount of WC particles is 0.1 wt%.

The adsorption theorem of surface active materials is considered, the effect of WC nanoparticles on the spreadability of Sn57.6Bi0.4Ag solder is analyzed; adsorption can be expressed as [25, 26]

$$\gamma_C^K = \gamma_0^K - RT\int_0^C \frac{\Gamma^k}{C} d_C, \tag{2}$$

where Γ^k is the amount of nanoparticles adsorbed per unit area of the molten solder k, c is the concentration of nanoparticles in the molten solder, R is the gas constant, T is the absolute temperature, γ_C^K is the surface energy per unit area of molten solder after nanoparticle adsorption, and γ_0^K is the surface energy per unit area of molten solder that is not adsorbed by nanoparticles. After adsorption, the surface energy of the molten solder in equilibrium is

$$\sum_K \gamma_C^K A_K = \sum_K \left(\gamma_0^K - RT\int_0^C \frac{\Gamma^k}{C} d_C \right) A_K, \tag{3}$$

where A_K is the surface area of the molten solder. When the adsorption amount Γ^k is positive, the surface energy of the molten solder on the right side of Eq. (3) is reduced. The WC particles decreased the surface energy of the molten Sn57.6Bi0.4Ag solder by adsorption and the spreadability of the Sn57.6Bi0.4Ag solder is improved. As shown in Fig. 3, the spreadability of Sn57.6Bi0.4Ag solder is improved by 0.025 wt% WC particles. However, the improvement of the spreadability is not obvious due to the small amount of WC. The spreadability is significantly improved when 0.05 wt% WC particles are added. The adsorption theorem indicates that the surface of liquid solder is affected by nanoparticles, 0.05–0.1 wt% of WC particles are positively adsorbed surface active substances and segregated on the surface of the liquid solder, which reduces the surface tension of the liquid solder and significantly improves the spreadability of the liquid Sn57.6Bi0.4Ag solder alloy. Van der Waals forces exist between the nanoparticles causing the particles to agglomerate with the increase of nano-WC content, which increases the viscosity of the liquid solder and the spreadability of

solder is deteriorated gradually [27]. The spreadability of Sn57.6Bi0.4Ag solder is improved by WC particles.

3.3 Microstructure

The microstructure of Sn57.6Bi0.4Ag–*x*WC (*x* = 0, 0.1) is shown in Fig. 4, Sn57.6Bi0.4Ag solder alloy consists of white Bi-rich phase and black Sn-rich phase, showing a lamellar microstructure, the Sn-rich phases and the Bi-rich phases interlock with each other alternately. Ag_3Sn is found on the boundary of the Bi phase of Sn57.6Bi0.4Ag and Sn57.6Bi0.4Ag–0.1WC solder alloys, the sizes of the Ag_3Sn particles are less than 1 μm (Fig. 4). Due to the high melting point of WC particles, the particles are in the solid state during the reflow process. Therefore, the distribution of W represents the distribution of WC. The elemental mappings for Sn, Bi, Ag and W in the Sn57.6Bi0.4Ag–0.1WC solder are shown in Fig. 5; the results show that WC nanoparticles are evenly distributed in Sn57.6Bi0.4Ag solder alloys.

The average Sn phase spacing of Sn57.6Bi0.4Ag and Sn57.6Bi0.4Ag–0.1WC solder alloys is 2.9 ± 1 μm and 2.1 ± 0.5 μm, respectively. WC particles act as the nucleation sites during reflow, the lamellar microstructure of the Sn57.6Bi0.4Ag solder is refined due to the increase in the number of nucleation sites. WC particles locate at the grain boundaries of the Sn-rich and Bi-rich phases during solidification, and produce a pinning effect on the movement of grain boundaries, which inhibits the grain growth [28]. The relationship between the pinning force and the inclusions is expressed as [17]

$$F_z = n_s \pi r \gamma, \tag{4}$$

where F_z is the pinning force of the inclusions, n_s is the number of inclusions per unit area, r is the radius of the particles, γ is the surface tension of the grain boundary. The number of particles per unit area in Sn57.6Bi0.4Ag solder alloy are increased by 0.1 wt% WC particles, the pinning force is enhanced, the growth of the Sn phase and the Bi phase is limited and the size of the Sn-rich and Bi-rich grains is refined.

3.4 Interfacial reaction

The interfacial morphologies of Sn57.6Bi0.4Ag/Cu and Sn57.6Bi0.4Ag–0.1WC/Cu joints are illustrated in Fig. 6. The Sn57.6Bi0.4Ag/Cu IMC has a uniform thickness of 2.0 μm (Fig. 7), partly grows towards the inside of the solder; the composition of the Sn57.6Bi0.4Ag/Cu IMC is Cu_6Sn_5. Figure 6b shows the interfacial IMC of Sn57.6Bi0.4Ag–0.1WC/Cu solder joint, the IMC thickness is relatively thin, and the interface is uneven adjacent to the solder. The IMC morphology of Sn57.6Bi0.4Ag/Cu and Sn57.6Bi0.4Ag–0.1WC/Cu solder joints aged at 100 °C for 250 h is flat and scallop-like, respectively. The IMC thickness of Sn57.6Bi0.4Ag/Cu and Sn57.6Bi0.4Ag–0.1WC/Cu is 3.4 μm and 2.75 μm, respectively. After 500 h aging, Bi phase is not being formed in the Sn57.6Bi0.4Ag/Cu and Sn57.6Bi0.4Ag–0.1WC/Cu IMCs, the IMC morphology of them has not changed, and the thickness of them is measured as 3.9 μm and 3.6 μm. The IMC layers of Sn57.6Bi0.4Ag/Cu and Sn57.6Bi0.4Ag–0.1WC/Cu show a two-layer structure after aging at 100 °C for 1000 h. A dark-colored layer inclusion is generated between Cu_6Sn_5 layer and Cu sheet, which is identified as Cu_3Sn as shown in Fig. 8. The IMC layer thickness in the Sn57.6Bi0.4Ag/Cu joint is about 4.6 μm.

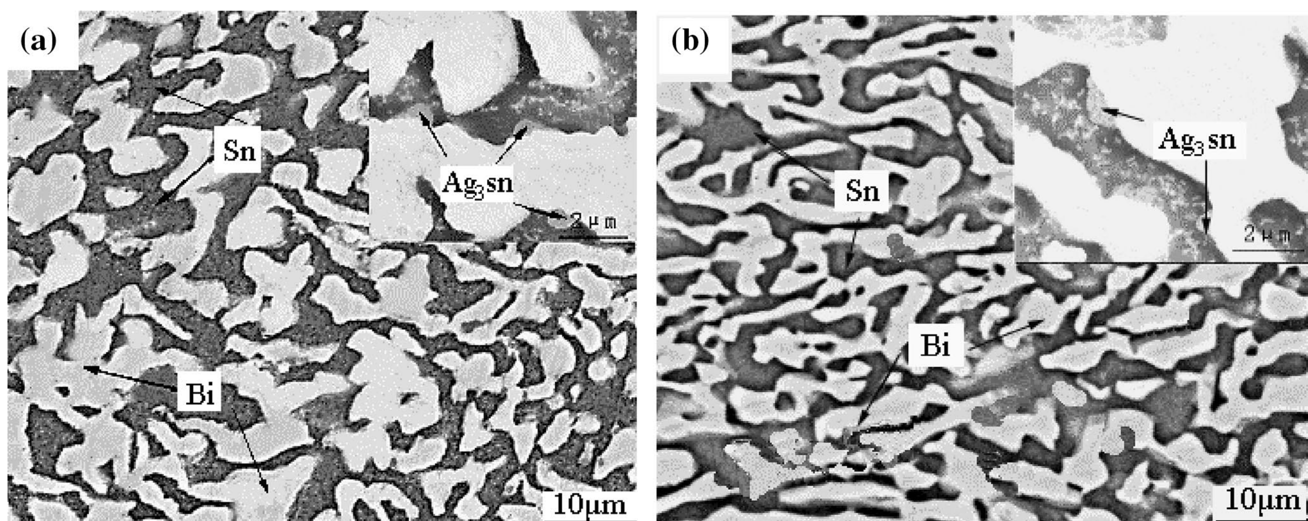

Fig. 4 Microstructure of **a** Sn57.6Bi0.4Ag solder and **b** Sn57.6Bi0.4Ag–0.1WC solder

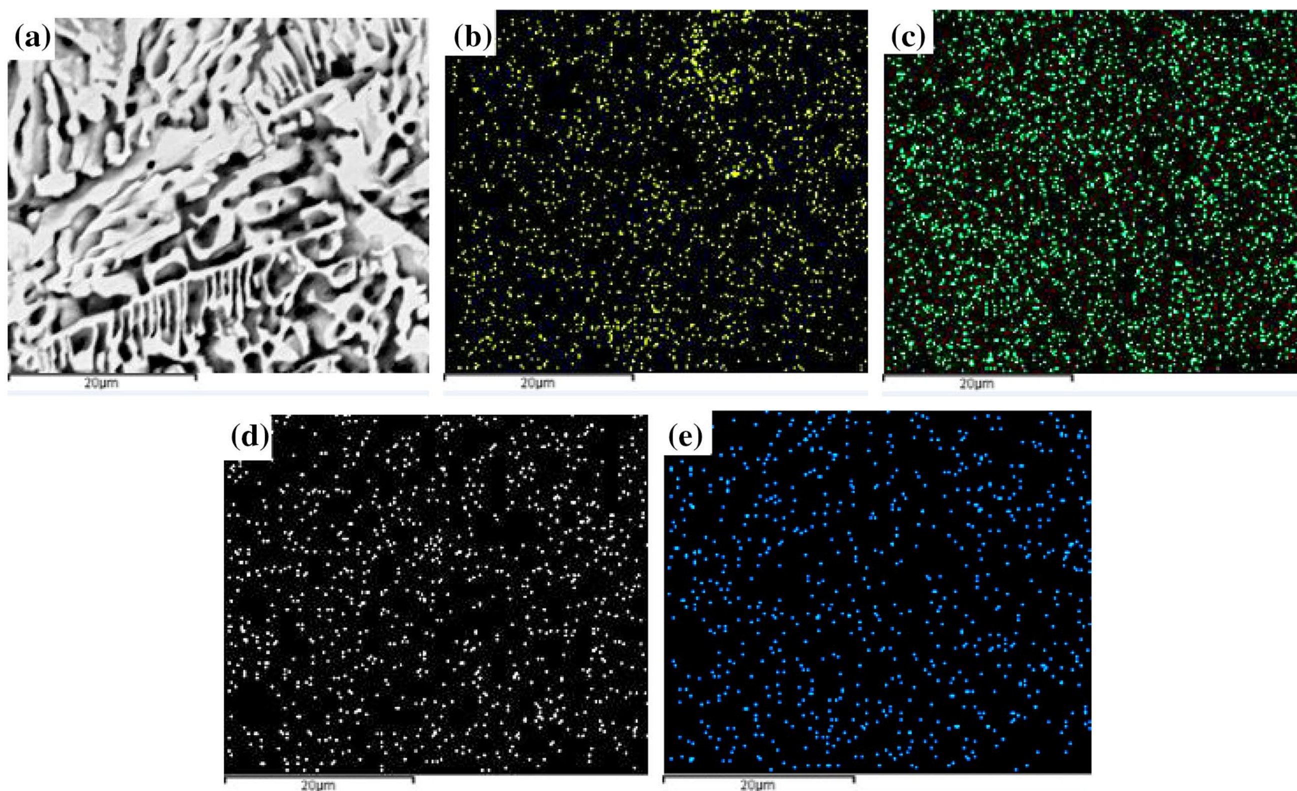

Fig. 5 EDS results of Sn57.6Bi0.4Ag–0.1WC solder: **a** SEM image, mapping for **b** Sn, **c** Bi, **d** Ag and **e** W

The IMC layer of Sn57.6Bi0.4Ag–0.1WC/Cu is relatively flat, and the IMC thickness of Sn57.6Bi0.4Ag–0.1WC/Cu is thinner than that of Sn57.6Bi0.4Ag/Cu aged at 100 °C for 1000 h.

The IMC thickness of the Sn57.6Bi0.4Ag–0.1WC/Cu joint is lower than that of Sn57.6Bi0.4Ag/Cu joint during the reflow process. According to the adsorption theory, the surface energy of Cu_6Sn_5 IMC can be expressed as

$$\sum_N \gamma_c^N S_N = \sum_N \left(\gamma_0^N - RT \int_0^c \frac{\Pi^N}{c} d_c \right) S_N = \sum_N \gamma_0^N S_N - RT \sum_N S_N \cdot \int_0^c \frac{\Pi^N}{c} d_c, \tag{5}$$

where c is the nano-WC particle content, γ^N is the surface energy of Cu_6Sn_5 grain, γ_0^N is the surface energy of Cu_6Sn_5 grain without adsorbing nanoparticles, γ_c^N is the surface energy of Cu_6Sn_5 grains that have adsorbed nanoparticles, S_N is the surface area of Cu_6Sn_5, Π^N is the adsorption amount of nanoparticles on the surface of Cu_6Sn_5, R is the gas constant, and T is the absolute temperature. The increase of Π^N leads to an increase in the value of the phase-integral $\int_0^c \frac{\Pi^N}{c} d_c$ in Eq. (5), and the surface energy of Cu_6Sn_5 is reduced. Gibbs's theory proves that reducing the surface energy of grains leads to slower growth of grains [29]. Adding WC particles to the Sn57.6Bi0.4Ag solder causes adsorption, the growth rate of Cu_6Sn_5 is slowed down. In addition, the growth of the IMC depends on the interdiffusion of Cu atoms and Sn atoms at the interface position; the WC particles located at the grain boundary and inside the crystal hinder the diffusion of Cu atoms and Sn atoms; the growth rate of the interface IMC is reduced [30].

During the aging process, the IMC layer thicknesses of Sn57.6Bi0.4Ag/Cu and Sn57.6Bi0.4Ag–0.1WC/Cu solder joints are linearly related to the square root of aging time according to Arrhenius equation [31, 32]:

$$d_t = d_0 + Dt^{1/2}, \tag{6}$$

where d_t is the average thickness of the IMC layer at aging time t, d_0 is the initial thickness, and D is the diffusion coefficient, so the growth rate of IMC layer thickness of Sn57.6Bi0.4Ag/Cu and Sn57.6Bi0.4Ag–0.1WC/Cu solder joints is first fast and then slow, the IMC thickness of the Sn57.6Bi0.4Ag–0.1WC/Cu joint is relatively thinner than that of the Sn57.6Bi0.4Ag/Cu joint after aging at 100 °C for 250–1000 h.

Cu_3Sn is found at Sn57.6Bi0.4Ag/Cu and Sn57.6Bi0.4Ag–0.1WC/Cu joints between Cu_6Sn_5 layer

Fig. 6 Cross-sectional morphologies of **a** Sn57.6Bi0.4Ag/Cu and **b** Sn57.6Bi0.4Ag–0.1WC/Cu solder joints after aging treatment with magnified views of **c** Sn57.6Bi0.4Ag/Cu, 100 °C, 1000 h and **d** Sn57.6Bi0.4Ag–0.1WC/Cu, 100 °C, 1000 h solder joints

and Cu sheet after 1000 h aging as shown in Fig. 6c, d. Cu_3Sn IMCs layer is mainly nucleated and grown by atomic solid-state reaction in a solid-state process, and it is formed according to the following equation:

$$9Cu + Cu_6Sn_5 = 5Cu_3Sn. \quad (7)$$

WC has a higher melting point of about 2870 °C, a smaller particle size and the chemical property of it is stable. It does not react with the solder alloy to form a new phase during the aging process.

3.5 Shear strength

Figure 9 illustrates the average shear strength of Sn57.6Bi0.4Ag/Cu and Sn57.6Bi0.4Ag–0.1WC/Cu solder joints after aging at 100 °C for 250–1000 h. The shear strength of Sn57.6Bi0.4Ag/Cu and Sn57.6Bi0.4Ag–0.1WC/Cu solder joints shows a downward trend as the aging time increases. The shear strength of Sn57.6Bi0.4Ag/Cu solder joint is 113.6 MPa, it is decreased to 96.2 MPa after aging for 250 h. As the aging time increases, the mechanical properties of Sn57.6Bi0.4Ag/Cu continue to decline, the minimum shear strength of Sn57.6Bi0.4Ag/Cu solder joint 87.1 MPa is obtained after aging at 100 °C for 1000 h. The similar

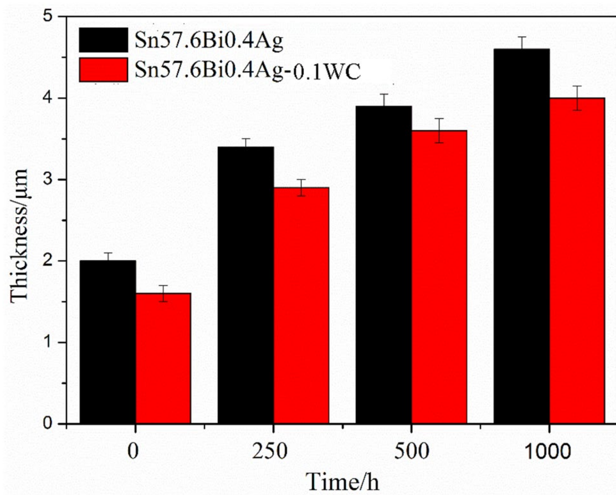

Fig. 7 Average thicknesses of the interfacial IMCs between Sn57.6Bi0.4Ag–xWC ($x=0$, 0.1) solder and Cu substrate after 250–1000 h aging

trends are observed in the Sn57.6Bi0.4Ag–0.1WC/Cu solder joint, and the shear strength of Sn57.6Bi0.4Ag–0.1WC/Cu solder joint is 127.6 MPa, it is decreased to 92.2 MPa under 100 °C for 1000 h. Figure 10a, c shows the fracture of Sn57.6Bi0.4Ag/Cu and Sn57.6Bi0.4Ag–0.1WC/Cu solder joints; the fracture paths are entirely inside the solder region. The shear fracture surface of Sn57.6Bi0.4Ag/Cu solder joint is relatively smooth, and obvious slip zone appears on the fracture surface as shown in Fig. 10b. The shear fracture surface of Sn57.6Bi0.4Ag–0.1WC/Cu solder joint is rough; some dimples appear on the fracture surface (Fig. 10d).

The shear strength of Sn57.6Bi0.4Ag–0.1WC/Cu solder joint is higher than that of Sn57.6Bi0.4Ag/Cu after reflow. The dislocation movement is hindered by refined microstructure of Sn57.6Bi0.4Ag/Cu solder joint, the shear strength of Sn57.6Bi0.4Ag–0.1WC/Cu solder joint is improved [33]. The shear strength of the solder joints is related to grain size, the driving force of grain boundary movement is inversely proportional to the curvature radius of the grain boundary during grain growth. As the grain grows during aging, the curvature radius of the grain becomes larger and the driving force of grain boundary motion is gradually reduced. The shear strength of Sn57.6Bi0.4Ag/Cu and Sn57.6Bi0.4Ag–0.1WC/Cu solder joints decreases more significantly in the early period and slowly in the later period. WC particles will bring stress concentration and lead to holes; dimple-like fracture is formed by the gradual growth and collection of holes under the action of shearing force. The ductility of the Sn57.6Bi0.4Ag–0.1WC/Cu solder joint is better compared with the Sn57.6Bi0.4Ag/Cu solder joint.

The shear fracture surface of Sn57.6Bi0.4Ag/Cu and Sn57.6Bi0.4Ag–0.1WC/Cu solder joints aged at 1000 h as shown in Fig. 11. Relatively dark fracture features appear on the local surface of Sn57.6Bi0.4Ag/Cu solder joints as shown in the upper right corner of Fig. 11a. The concentration of Cu in this area is significantly increased, and the concentrations of Sn and Bi elements are reduced as shown in Fig. 11b, the darker fracture region occurs at the IMC of Sn57.6Bi0.4Ag/

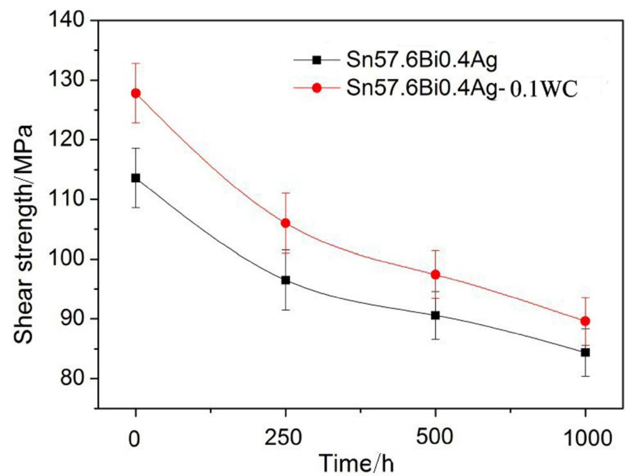

Fig. 9 Shear strengths of Sn57.6Bi0.4Ag/Cu and Sn57.6Bi0.4Ag–0.1WC/Cu solder joints after aging for various times

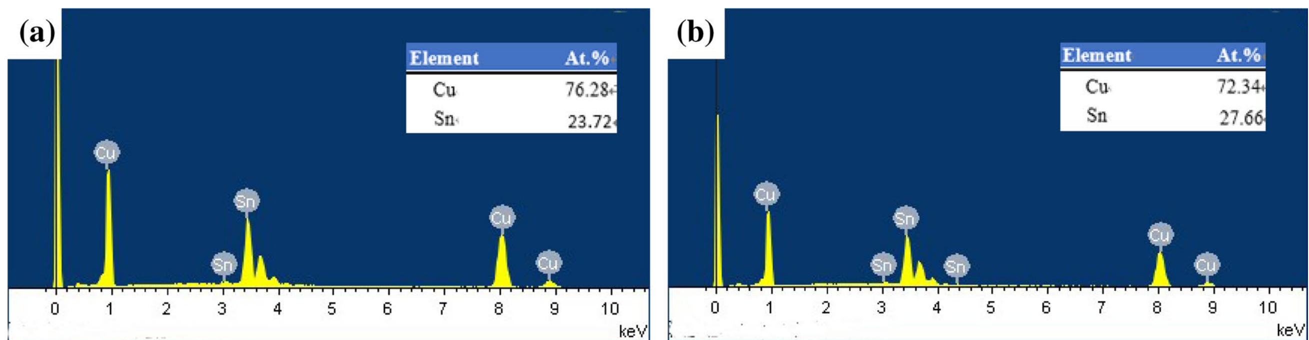

Fig. 8 EDS results of the IMC layer in Sn57.6Bi0.4Ag/Cu and Sn57.6Bi0.4Ag–0.1WC/Cu joint as presented in Fig. 6c, d

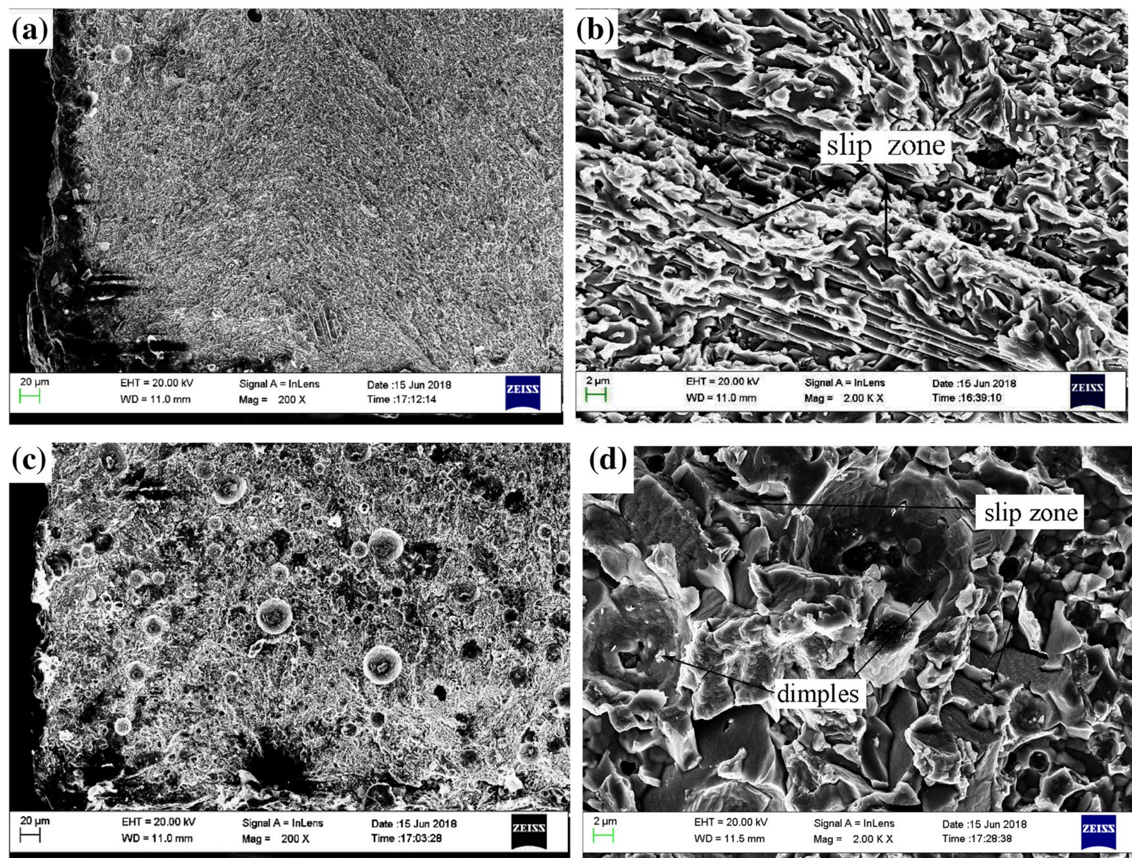

Fig. 10 Shear fracture surfaces of **a** Sn57.6Bi0.4Ag/Cu, **b** Sn57.6Bi0.4Ag–0.1WC/Cu solder joints with magnified views of the as-reflowed, **c** Sn57.6Bi0.4Ag/Cu and **d** Sn57.6Bi0.4Ag–0.1WC/Cu solder joints

Cu and the entire shear fracture of the Sn57.6Bi0.4Ag/Cu solder joint occurs in the solder and IMC mixing region. The fracture surface of Sn57.6Bi0.4Ag/Cu solder joint has no obvious plastic deformation and shows brittle fracture characteristics. Figure 11c shows the shear fracture surface of Sn57.6Bi0.4Ag–0.1WC/Cu solder joint aged at 1000 h, and the fracture characteristics of Sn57.6Bi0.4Ag–0.1WC/Cu solder joints show plastic fracture characteristics. Many dimples appear on the fracture surface and the diameter of the dimples is smaller than that of Sn57.6Bi0.4Ag–0.1WC/Cu solder joint without aging. The dimples become smaller during the aging process indicating that the ductility is reduced and the Sn57.6Bi0.4Ag/Cu solder joints are more brittle than Sn57.6Bi0.4Ag–0.1WC/Cu solder joints aged at 1000 h. In general, WC particles improve the shear strength and ductility of Sn57.6Bi0.4Ag/Cu solder joints by refining the microstructure.

4 Conclusions

The Sn57.6Bi0.4Ag–*x*WC/Cu ($x = 0$, 0.025, 0.050, 0.100, 0.200) solder joints have been prepared. The effects of WC nanoparticles on the spreadability, microstructure, IMC growth and mechanical properties of Sn57.6Bi0.4Ag/Cu solder joints are investigated. The conclusions are as follows:

1. The spreadability of Sn57.6Bi0.4Ag solder is improved by WC particles. The spreading area of Sn57.6Bi0.4Ag solder increases first and decreases with increasing WC content next; when the addition amount of WC particles is 0.1 wt%, Sn57.6Bi0.4Ag solder gets relatively optimal spreadability.
2. The microstructure of Sn57.6Bi0.4Ag solder alloy is refined by 0.1 wt% WC particle. The IMC thick-

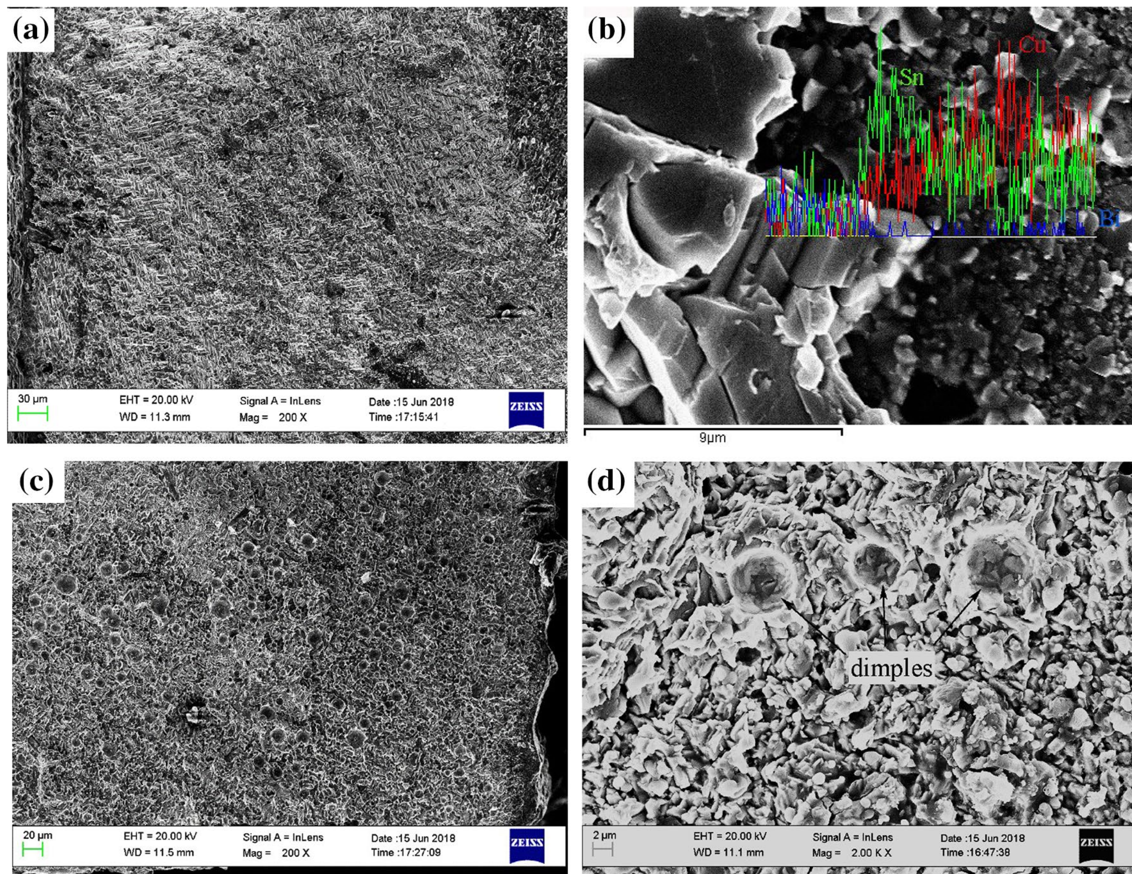

Fig. 11 Shear fracture surfaces of **a** Sn57.6Bi0.4Ag/Cu, 100 °C, 1000 h and **b** Sn57.6Bi0.4Ag–0.1WC/Cu, 100 °C, 1000 h solder joints with magnified views of **c** Sn57.6Bi0.4Ag/Cu, 100 °C, 1000 h and **d** Sn57.6Bi0.4Ag–0.1WC/Cu, 100 °C, 1000 h solder joints

ness of Sn57.6Bi0.4Ag/Cu joint is thicker than that of Sn57.6Bi0.4Ag–0.1WC/Cu joint during the reflow process, and the formation of Sn57.6Bi0.4Ag/Cu solder joint IMC is suppressed by WC particles.

3. The shear property of Sn57.6Bi0.4Ag/Cu solder joint is improved by WC particles, and the generation of dimples is promoted by WC particles. The shear strength and ductility of Sn57.6Bi0.4Ag–0.1WC/Cu solder joints are higher than those of Sn57.6B.4Ag/Cu solder joints during the aging process.

Acknowledgements This research was financially supported by the National Natural Science Foundation of China (Grant nos. 51865006, 51505040, and 51401037).

References

1. H.R. Kotadia, P.D. Howes, S.H. Mannan, A review: on the development of low melting temperature Pb-free solders. Microelectron. Reliab. **54**(6–7), 1253–1273 (2014)
2. C. Li, X. Hu, X. Jiang, Interfacial reaction and microstructure between the Sn3Ag0.5Cu solder and Cu–Co dual-phase substrate. Appl. Phys. A **124**(7), 484 (2018)
3. L. Zhang, P. Dou, W. Wang, Sn–Cu nanotubes enveloped in three-dimensional interconnected polyaniline hydrogel framework as binder-free anode for lithium-ion battery. Appl. Surf. Sci. **423**, 245–254 (2017)
4. S. Delsante, R. Novakovic, G. Borzone. Synthesis, characterization and thermal stability of SnAg and SnAgCu nanoparticles. J. Alloys Compd. **747**, 385–393 (2018)
5. M.Y. Rekha, A. Kamboj, C. Srivastava, Electrochemical behavior of SnZn-graphene oxide composite coatings. Thin Solid Films **636**, 593–601 (2017)

6. J.W. Yoon, B.I. Noh, S.B. Jung, Comparison of interfacial stability of Pb-free solders (Sn-3.5 Ag, Sn-3.5 Ag-0.7 Cu, and Sn-0.7 Cu) on ENIG-plated Cu during aging. IEEE Trans. Compon. Packag. Technol. **33**(1), 64–70 (2010)
7. Q.K. Zhang, Q.S. Zhu, H.F. Zou, Fatigue fracture mechanisms of Cu/lead-free solders interfaces. Mater. Sci. Eng. A **527**(6), 1367–1376 (2010)
8. J.H. Park, J.H. Lee, Y.H. Lee, Reaction characteristics of the Au-Sn solder with under-bump metallurgy layers in optoelectronic packages. J. Electron. Mater. **31**(11), 1175–1180 (2002)
9. Y. Li, Y.C. Chan, Effect of silver (Ag) nanoparticle size on the microstructure and mechanical properties of Sn58Bi–Ag composite solders. J. Alloys Compd. **645**, 566–576 (2015)
10. H. Sun, Y.C. Chan, F. Wu, Influence of the aggregated Ag_3Sn on the improvement of electromigration phenomenon in the doped Sn58Bi solder joints. J. Mater. Sci. Mater. Electron. **26**(7), 5129–5134 (2015)
11. H. Sun, Q. Li, Y.C. Chan, A study of Ag additive methods by comparing mechanical properties between Sn57.6Bi0.4Ag and 0.4 wt% nano-Ag-doped Sn58Bi BGA solder joints. J. Mater. Sci. Mater. Electron. **25**(10), 4380–4390 (2014)
12. C. Kanchanomai, Y. Mutoh, Low-cycle fatigue prediction model for Pb-Free Solder 96.5Sn3.5Ag. J. Electron. Mater. **33**(4), 329–333 (2004)
13. L. Zhang, J. Han, C. He, Effect of Zn on properties and microstructure of SnAgCu alloy. J. Mater. Sci. Mater. Electron. **23**(11), 1950–1956 (2012)
14. L. Shen, Z.Y. Tan, Z. Chen, Nanoindentation study on the creep resistance of SnBi solder alloy with reactive nano-metallic fillers. Mater. Sci. Eng. A **561**, 232–238 (2013)
15. J.W. Yoon, S.B. Jung, Reliability studies of Sn–9Zn/Cu solder joints with aging treatment. J. Alloys Compd. **407**(1–2), 141–149 (2006)
16. S.T. Oh, J.H. Lee, Microstructural, wetting, and mechanical characteristics of Sn-57.6 Bi-0.4 Ag alloys doped with metal–organic compounds. Electron. Mater. Lett. **10**(2), 473–478 (2014)
17. Y. Li, K. Luo, A.B.Y. Lim, Improving the mechanical performance of Sn57.6Bi0.4Ag solder joints on Au/Ni/Cu pads during aging and electromigration through the addition of tungsten (W) nanoparticle reinforcement. Mater. Sci. Eng. A **669**, 291–303 (2016)
18. H. Sun, Y.C. Chan, F. Wu, Effect of CNTs and Ni coated CNTs on the mechanical performance of Sn57.6Bi0.4Ag BGA solder joints. Mater. Sci. Eng. A **656**, 249–255 (2016)
19. T. Hu, Y. Li, Y.C. Chan, Effect of nano Al_2O_3, particles doping on electromigration and mechanical properties of Sn–58Bi solder joints. Microelectron. Reliab. **55**(8), 1226–1233 (2015)
20. D.H. Tran-Nguyen, D. Jewell, D.J. Fray. Electrochemical preparation of tungsten, tungsten carbide and cemented tungsten carbide. Miner. Process. Extr. Metall. **123**(1), 53–60 (2014)
21. M. Sabzi, S.H.M. Anijdan, M. Ghobeiti-Hasab, Sintering variables optimization, microstructural evolution and physical properties enhancement of nano-WC ceramics. J. Alloys Compd. **766**(25), 672–677 (2018)
22. T. Fouzder, I. Shafiq, Y.C. Chan, Influence of $SrTiO_3$ nanoparticles on the microstructure and shear strength of Sn–Ag–Cu solder on Au/Ni metallized Cu pads. J. Alloys Compd. **509**(5), 1885–1892 (2011)
23. L.C. Tsao, An investigation of microstructure and mechanical properties of novel Sn3.5Ag0.5Cu–$XTiO_2$ composite solders as functions of alloy composition and cooling rate. Mater. Sci. Eng. A **529**(33), 41–48 (2011)
24. Y. Huang, Z. Xiu, G. Wu et al., Sn3.0Ag0.5Cu nanocomposite solders reinforced by graphene nanosheets. J. Mater. Sci. Mater. Electron. **27**(7), 1–7 (2016)
25. J. Shen, Y.C. Chan, Effect of metal/ceramic nanoparticle-doped fluxes on the wettability between Sn–Ag–Cu solder and a Cu layer. J. Alloys Compd. **477**(1–2), 909–914 (2009)
26. J. Shen, Y.C. Chan, Research advances in nano-composite solders. Microelectron. Reliab. **49**(3), 223–234 (2009)
27. F. Yang, L. Zhang, Z. Liu, Effects of CuZnAl particles on properties and microstructure of Sn-58Bi solder. Materials **10**(5), 1–10 (2017)
28. Y. Liu, H. Fu, F. Sun, Microstructure and mechanical properties of as-reflowed Sn58Bi composite solder pastes. J. Mater. Process. Technol. **238**, 290–296 (2016)
29. Y. Tang, G.Y. Li, Y.C. Pan, Influence of TiO_2 nanoparticles on IMC growth in Sn–3.0 Ag–0.5 Cu–$xTiO_2$ solder joints in reflow process. J. Alloys Compd. **554**, 195–203 (2013)
30. S. Xu, Y.C. Chan, K. Zhang, Interfacial intermetallic growth and mechanical properties of carbon nanotubes reinforced Sn3.5Ag0.5Cu solder joint under current stressing. J. Alloys Compd. **595**, 92–102 (2014)
31. X. Hu, T. Xu, X. Jiang, Effects of post-reflow cooling rate and thermal aging on growth behavior of interfacial intermetallic compound between SAC305 solder and Cu substrate. Appl. Phys. A **122**(4), 1–10 (2016)
32. A. Paul, C. Ghosh, W.J. Boettinger, Growth mechanism of phases, Kirkendall voids, marker plane position, and indication of the relative mobilities of the species in the interdiffusion zone. J. Mater. Sci. Mater. Electron. **22**, 833–837 (2011)
33. L. Yang, J. Ge, Y. Zhang, Effect of $BaTiO_3$ on the microstructure and mechanical properties of Sn1.0Ag0.5Cu lead-free solder. J. Mater. Sci. Mater. Electron. **26**(1), 613–619 (2015)